Safety-Critical Generalized Predictive Control for PMSM Drives Based on Control Barrier Function

1st Zhongkun Cao
College of Automation Engineering, Shanghai University of Electric Power
Shanghai, China
caozhongkun@mail.shiep.edu.cn

2nd Jianliang Mao
College of Automation Engineering, Shanghai University of Electric Power
Shanghai, China
jl_mao@shiep.edu.cn

3rd Muhammad Irshad Khan
College of Automation Engineering, Shanghai University of Electric Power
Shanghai, China
irshadnawab@nuaa.edu.cn

4th Xin Dong
College of Automation Engineering, Shanghai University of Electric Power
Shanghai, China
xxddong@shiep.edu.cn

5th Chuanlin Zhang
College of Automation Engineering, Shanghai University of Electric Power
Shanghai, China
clzhang@shiep.edu.cn

***Abstract*—This paper presents a novel safety-critical generalized predictive control (SCGPC) strategy for speed regulation of permanent synchronous motor (PMSM) drives with a non-cascade structure. The proposed approach incorporates a robust control barrier function (RCBF) to explicitly consider the current constraint, addressing the constraint deviation problem caused by disturbances through a disturbance estimation and compensation technique. By solving an optimization problem, the RCBF-based current constraint mechanism and the generalized predictive control (GPC)-based speed controller are unified, combining the advantages of GPC and model predictive control (MPC). The integrated approach achieves efficient calculation without imposing a high computational burden, while simultaneously ensuring fast-tracking of the desired speed and strict adherence to current constraint. Both simulation and experimental results confirm the effectiveness of the proposed approach when compared to traditional MPC and GPC methods.**

***Index Terms*—PMSM speed regulation, generalized predictive control, control barrier function, current constraint.**

I. Introduction

Permanent magnet synchronous motors (PMSMs) have been widely adopted in various industrial applications due to their high efficiency, compact structure and high power density [1]–[3]. Although the control strategies for PMSM drives have been extensively researched and yielded fruitful results, achieving high performance and high-precision control for the PMSM drives subject to disturbances and safety constraint problems still remains a challenging task.

It is widely acknowledged that field-oriented control (FOC) employing the cascade structure is a commonly used and effective approach for controlling permanent magnet synchronous motors (PMSMs) [4]. However, to prevent undesired overshoot, the dynamic performance of the closed-loop system is usually restricted to a certain extent. To tackle this issue, the non-cascade control method is proposed in [5], [6], where the q-axis current loop is eliminated, enhancing the dynamic performance of the system. Despite its advantages, the q-axis current is no longer constrained by a reference value [5], thereby introducing current safety protection concerns.

As an optimal control approach, MPC has received increasing attention thanks to its intuitive concept, straightforward design and ability to handle the constraint problem [7]. Consequently, extensive research has been conducted on the application of the MPC method to PMSM drive systems, leading to fruitful achievements [8]. As a fast-sampling system, PMSM requires the control algorithm to be computed quickly within each sampling period. Real-time implementation of MPC, on the other hand, necessitates a lot of computing power during each sampling period [9]. This makes it difficult for industrial processors with limited computing power to take full advantage of MPC.

As an alternative, the GPC approach is proposed in [10]. In contrast to MPC, GPC provides an offline receding optimization option for the predictive model based on continuous Taylor expansion, which significantly reduces the amount of computation that needs to be done [11]. However, it is important to note that this approach only provides an explicit optimal controller based on the designed performance index and does not tackle the constraint problem. Therefore, when applied to a PMSM speed regulation system with a non-cascade structure, the GPC approach allows fast-tracking of the desired speed reference signals but does not guarantee that the current is within the predefined safe range.

In recent years, the safety-critical control problem for nonlinear systems has gained significant attention in the control field. The control barrier function (CBF), as a powerful tool addressing the constrained control problem, has been broadly studied [12]–[15]. Specifically, the CBF has been applied to an automotive system for maintaining a safe following distance in [13]. In [15], the CBF has been applied to a robotic system for ensuring that the robot walks safely on a series of stepping

This work was supported in part by the National Natural Science Foundation of China under Grants 62173221 and 62203292. (*Corresponding author: Jianliang Mao.*)

stones. Furthermore, by combining the constructed CBF and the control Lyapunov function (CLF) into a quadratic problem (QP), the safety constraint problem and tracking performance objective are considered simultaneously in [16]. This achieves a comprehensive control option that aims to ensure the tracking objective as much as possible while satisfying safety constraints. It should be noted, nevertheless, that all the above CBF designs are based on undisturbed systems, thus rendering them less suitable for disturbed systems.

After a partial review of the above, motivated by the aforementioned CBF-CLF-based QP approaches in [16], a novel SCGPC method based on RCBF is investigated in this article. Firstly, a GPC-based speed controller is designed under a non-cascade structure to achieve fast tracking of the given reference signals in the presence of mismatched and matched disturbances. Secondly, a current constrained RCBF based on disturbance observer (DOB) is developed to achieve strict current safety control even in the presence of disturbances. Finally, a current safety-critical controller is presented by unifying the designed GPC-based speed controller and DOB-based RCBF into an optimization problem. The contributions of this paper are summarized as follows:

1) For speed regulation of PMSM drives, a novel SCGPC strategy is proposed under a non-cascade framework, which well integrates the merits of the GPC and MPC with a more efficient computation.
2) Inspired by the nominal CBF under the undisturbed systems, a DOB-based current constrained RCBF is developed to realize strict current safety-critical control even under disturbances.

II. Problem Formulation

A. Dynamic Model of PMSM Drives

The dynamic model of a surface-mounted PMSM in the d-q coordinate system is explicitly expressed as follows:

$$\begin{cases} \dot{\omega} = (1.5 n_p \psi_f i_q - B_m \omega - T_L)/J, \\ \dot{i_d} = (-R_s i_d + n_p \omega L_s i_q + u_d)/L_s, \\ \dot{i_q} = (-R_s i_q - n_p \omega L_s i_d - n_p \psi_f \omega + u_q)/L_s \end{cases} \tag{1}$$

where ω is the mechanical angular velocity; T_L is the load torque; i_q and u_q are the stator current and voltage of the d-axis; i_d and u_d are the stator current and voltage of the q-axis; ψ_f is the rotor flux linkage; B_m is the viscous frictional coefficient; J is the rotor inertia; L_s is the stator resistance; n_p is the number of pole pairs.

Note that in this paper, the d-axis current loop still utilizes a PI controller and is assumed to be ideal tracking, with d-axis current reference i_d^* being set to zero, thus i_d = 0 is derived.

B. Control Objective

Define $x_1 = \omega_{\text{ref}} - \omega$ and $x_2 = \frac{1}{J}(-n_p \psi_f i_q + B_m \omega_{\text{ref}})$ as the system states, where ω_{ref} is the reference speed. With $i_d = 0$ in mind, the state-space model of (1) can be expressed by

$$\begin{cases} \dot{x}_1 = x_2 + f_1(\bar{x}) + d_1, \\ \dot{x}_2 = u + f_2(\bar{x}) + d_2 \end{cases} \tag{2}$$

where $u = -\frac{3 n_p \psi_f}{2 J L_s} u_q$ and x_1 are the system input and output; $\bar{x} = (x_1, x_2)^\top$; d_1 is treated as the mismatched lumped disturbance including load disturbance $\frac{T_L}{J}$ and model uncertainties of the mismatched channel; d_2 is regarded as the lumped disturbance of the matched channel; $f_1(\bar{x}) = -\frac{B_m}{J} x_1$ and $f_2(\bar{x}) = -\frac{3 n_p^2 \psi_f^2}{2 J L_s} x_1 - \frac{R_s}{L_s} x_2 + \frac{1}{J L_s}(R_s B_m + \frac{3}{2} n_p^2 \psi_f^2)\omega_{\text{ref}}$ are the known model dynamics.

Assumption 1: The matched and mismatched disturbances in system (2) satisfy the condition that $\sup\{|d_1|, |\dot{d}_1|, |d_2|\} \leq D$, where D is a positive constant.

Our control objective is to design a safety-critical controller $u(\bar{x}, t)$ for system (2), with two main objectives in mind:

1) Ensuring that the built closed-loop system can achieve an offset-free tracking of the desired speed signal to the greatest extent possible under mismatched and matched disturbances.
2) Keeping the stator current within the allowable range defined by the operational constraints such that safe and reliable operation can be achieved, even in the presence of disturbances.

III. Benchmark GPC Design

In this section, two higher-order sliding mode observers (HOSMOs) are first introduced to reconstruct the matched and mismatched disturbances in the system. Then, based on the obtained disturbance estimates, a nominal predictive model with disturbance compensation is established. Finally, with the receding-horizon optimization of the obtained predictive model in terms of the defined performance index, an optimal speed controller is presented.

A. Disturbance Observation

For the purpose of reconstructing matched and mismatched disturbances in system, two HOSMOs are built as follows [17]:

$$d_1 : \begin{cases} \dot{w}_{1,0} = x_2 + f_1(\bar{x}) + \vartheta_{1,1}, \dot{w}_{1,i} = \vartheta_{1,i+1}, \\ \hbar_{1,i} = w_{1,i} - \vartheta_{1,i}, i = 0, 1, 2, \\ \vartheta_{1,1} = -\ell_{1,0} \rho_1^{1/3} |\hbar_{1,0}|^{2/3} \operatorname{sign}(\hbar_{1,0}) + w_{1,1}, \\ \vartheta_{1,2} = -\ell_{1,1} \rho_1^{1/2} |\hbar_{1,1}|^{1/2} \operatorname{sign}(\hbar_{1,1}) + w_{1,2}, \\ \vartheta_{1,3} = -\ell_{1,2} \rho_1 \operatorname{sign}(\hbar_{1,2}); \end{cases} \tag{3}$$

$$d_2 : \begin{cases} \dot{w}_{2,0} = u_1 + f_2(\bar{x}) + \vartheta_{2,1}, \\ \dot{w}_{2,1} = \vartheta_{2,2}, \hbar_{2,i} = w_{2,i} - \vartheta_{2,i}, i = 0, 1, \\ \vartheta_{2,1} = -\ell_{2,0} \rho_2^{1/2} |\hbar_{2,0}|^{1/2} \operatorname{sign}(\hbar_{2,0}) + w_{2,1}, \\ \vartheta_{2,2} = -\ell_{2,1} \lambda_2 \operatorname{sign}(\hbar_{2,1}) \end{cases} \tag{4}$$

where $w_{i,0}$ are the estimates of x_i; $w_{1,1}$, $w_{1,2}$ and $w_{2,1}$ are the estimates of d, $\dot{d}_1$ and d_2, respectively; $\vartheta_{i,0} = x_i$; $\vartheta_{2,i}$, $\hbar_{1,j}$ and $\hbar_{2,i-1}$ are the auxiliary states; $\ell_{1,j}$, $\ell_{2,i-1}$, and ρ_i are the positive gains for $i = 1, 2$, $j = 0, 1, 2$.

Define $\varepsilon_{i,0} = w_{i,0} - x_i$, $\varepsilon_{i,1} = w_{i,1} - d_i$ and $\varepsilon_{1,2} = w_{1,2} - \dot{d}_1$ as estimation errors ($i = 1, 2$).

B. Controller Design

First of all, assuming that the system disturbances are exactly available, one can naturally obtain the steady-state reference signals for system (2) as

$$\begin{cases} x_1^* = 0,\ x_2^* = -d_1, \\ u^* = -\dot{x}_2^* - f_2(\bar{x}^*) - d_2 \end{cases} \tag{5}$$

where $\bar{x}^* = (x_1^*, x_2^*)^\top$, x_1^*, x_2^* and u^* are the steady values of x_1, x_2 and u, respectively.

1) Steady-State Signal Construction: It should be noted that (5) is not implementable since it relies on the availability of disturbances. Define $\hat{\bar{x}}^* = (\hat{x}_1^*, \hat{x}_2^*)^\top$, by substituting the disturbance estimations $w_{1,1}$, $w_{1,2}$ and $w_{2,1}$ into (5), the implementable steady-state signals can be formulated as

$$\begin{cases} \hat{x}_1^* = 0,\ \hat{x}_2^* = -w_{1,1}, \\ \hat{u}^* = -w_{1,2} - f_2(\hat{\bar{x}}^*) - w_{2,1}. \end{cases} \tag{6}$$

2) Receding-Horizon Optimization: Define $\hat{\eta}_\omega = x_1 - \hat{x}_1^*$, $\hat{\eta}_q = x_2 - \hat{x}_2^*$ and $\hat{v}_q = u - \hat{u}^*$ as the available system errors and $\hat{\eta}_\alpha = [\hat{\eta}_\omega, \hat{\eta}_q]^\top$. By ignoring the estimation errors, a concise nominal error-oriented system model can be established as follows:

$$\dot{\hat{\eta}}_\alpha = A\hat{\eta}_\alpha + B\hat{v}_q, \tag{7}$$

where A and B are the controllable standard matrix pairs.

With the control order chosen as 0 (see [18] for details), the future output of the system $\tilde{\eta}_\omega(t+\tau)$ at a horizon τ can be predicted by the continuous Taylor expansion along nominal model (7) as

$$\tilde{\eta}_\omega(t+\tau) \doteq \hat{\eta}_\omega + \tau\hat{\eta}_q + \frac{\tau^2}{2!}\hat{v}_q = \mathcal{H}\hat{\eta}_\alpha + \frac{\tau^2}{2!}\hat{v}_q \tag{8}$$

where $\mathcal{H} = [1, \tau]$, $\tau > 0$.

To achieve optimal convergence of the tracking errors to zero, the cost function to be optimized is designed as follows

$$\hat{J}_\alpha(t) = \frac{1}{2}\int_0^T \hat{\eta}_\omega(t+\tau)^2 d\tau, \tag{9}$$

where $T > 0$ is the prediction horizon.

According to [6], by minimizing the performance index $\hat{J}_\alpha$, the following optimal controller can be easily attained as

$$u = -\frac{k_1^*}{T^2}\hat{\eta}_\omega - \frac{k_2^*}{T}\hat{\eta}_q + \hat{u}^*. \tag{10}$$

where k_1^* and k_2^* are the positive gains.

Remark 1: As presented in (10), the structure of the designed GPC-based speed controller is quite simple. It consists of a linear feedback loop based on steady-state signals and a feedforward compensation loop based on the known model dynamics and disturbance estimates. In addition, the parameter tuning procedure of the designed controller is also fairly straightforward. Specifically, the control gains k_1^* and k_2^* can be determined by conducting procedure (7)-(9), thus the system performance can be tuned simply by picking different T, where a lower T results in a faster response speed. Therefore, a practical solution for selecting T is to tune T from large to small until the desired control performance is obtained.

IV. Safety-Critical GPC Design

In this section, the current constrained CBF is first introduced to address the current safety constraint problem. Subsequently, to further tackle the problem of CBF constraint deviation caused by system disturbances, a new RCBF based on DOB is developed. Finally, by unifying the RCBF and the designed GPC-based speed controller into an optimization problem, a RCBF-based SCGPC controller is presented.

A. Baseline Control Barrier Function

Firstly, by rearranging system model (2), one can obtain

$$\dot{\bar{x}} = f(\bar{x}) + g_1(\bar{x})u + g_2(\bar{x})d \tag{11}$$

where $f(\bar{x}) = [x_2 + f_1(\bar{x}), f_2(\bar{x})]^\top$, $g_1(\bar{x}) = [0, 1]^\top$, $g_2(\bar{x}) = I_{2\times 2}$ and $d = [d_1, d_2]^\top$.

For system (11), by defining a set as the super-level set of a continuously differentiable function $h : \mathbb{R}^2 \to \mathbb{R}$ yields

$$\begin{aligned} \mathcal{C} &= \left\{\bar{x} \in \mathbb{R}^2 : h(\bar{x}) \geq 0\right\}, \\ \partial\mathcal{C} &= \left\{\bar{x} \in \mathbb{R}^2 : h(\bar{x}) = 0\right\}, \\ \operatorname{Int}\mathcal{C} &= \left\{\bar{x} \in \mathbb{R}^2 : h(\bar{x}) > 0\right\} \end{aligned} \tag{12}$$

where $\mathcal{C}$ is also called a safe set.

For practical application, the stator current of PMSM motor is physically constrained as follows:

$$\sqrt{i_q^2 + i_d^2} \leq I_{\max}, \tag{13}$$

where $I_{\max}$ is maximum allowable stator current.

With $i_d = 0$ in mind, the current constrained problem (13) can be simplified to

$$|i_q| \leq I_{\max}. \tag{14}$$

Based on system (2), the constraint (14) can be further transformed into the following state constrained problem

$$\underline{x}_2 \leq x_2 \leq \bar{x}_2, \tag{15}$$

where $\bar{x}_2 = \frac{1}{J}(n_p\psi_f I_{\max} + B_m\omega_{\text{ref}})$, $\underline{x}_2 = -\frac{1}{J}(n_p\psi_f I_{\max} - B_m\omega_{\text{ref}})$.

Inspired by [14], we choose the CBF candidate as follows:

$$\begin{cases} h_1^1(\bar{x}) = x_2 - \underline{x}_2, \\ h_1^2(\bar{x}) = \bar{x}_2 - x_2. \end{cases} \tag{16}$$

With the given $h_1^i(\bar{x})$, the corresponding safe set $\mathcal{C}_1^i \in \mathbb{R}^2$ defined by (17) can be obtained ($i = 1, 2$).

It should be note that $h_1^i(\bar{x})$ have relative degree order one, i.e., $L_g h_1^i(\bar{x}) \neq 0$, and satisfy $\frac{\partial h_1^i(\bar{x})}{\partial \bar{x}}(\bar{x}) \neq 0$ when $h_1^i(\bar{x}) = 0$. Thus, one can easily learn from [16] that $h_1^i(\bar{x})$ are valid CBFs. Furthermore, according to the *Corollary* 2 in [19], one can get that if the initial state of system x_2 satisfies $x_2 \in \mathcal{C}_1^1 \cap \mathcal{C}_1^2$, then for any locally Lipschitz continuous feedback controller as

$$\begin{aligned} u(\bar{x}) \in \big\{u \in \mathbb{R} \mid &: L_f h_1^i(\bar{x}) + L_{g1} h_1^i(\bar{x})u + L_{g2} h_1^i(\bar{x})d \\ &+\alpha\left(h_1^i(\bar{x})\right) \geq 0\big\}, \end{aligned} \tag{17}$$

the result that x_2 is in safe sets $\mathcal{C}_1^i$ at all times can be guaranteed, i.e., $x_2(t) \in \mathcal{C}_1^1 \cap \mathcal{C}_1^2$, $\forall t \in [0, \infty)$ holds, which also

means that the objective of current constraint can be reached by (17), where $L_f h_1^i$, $L_{g1} h_1^i$ and $L_{g2} h_1^i$ are Lie derivatives [20], α is an extended class K_∞ function.

B. Robust Control Barrier Function

Note that (17) is not implementable since it depends on the availability of disturbances. If the disturbances in (17) are not compensated, a current constraint deviation problem will naturally arise. However, even with the adoption of DOB for feedforward compensation, strict current constraint can still not be ensured due to the presence of estimation errors. To address these issues, a new RCBF is proposed below.

At first, with *Assumption* 1 in mind, it is a logical fact is that with a suitable choice of HOSMO gains there exists an upper bound on the estimation errors for the designed HOSMOs, i.e., there exists a bounded constant Γ satisfying $\sup\{|\varepsilon_{1,1}|, |\varepsilon_{2,1}|\} \leq \Gamma$. Based on this deduction, by letting $\alpha(\cdot) = \lambda(\cdot)$, where λ is positive constant, one can reformulate (17) as follows

$$u(\bar{x}) \in \Big\{ u \in \mathbb{R} \,|\colon L_f h_1^i(\bar{x}) + L_{g1} h_1^i(\bar{x}) u + L_{g2} h_1^i(\bar{x}) \hat{d} - L_{g2} h_1^i(\bar{x})(\hat{d} - d) + \lambda h_1^i(\bar{x}) \geq 0 \Big\}, \tag{18}$$

where $\hat{d} = [w_{1,1}, w_{2,1}]^\top$, $d = [d_1, d_2]^\top$.

Furthermore, by replacing the estimation errors $(\hat{d} - d)$ in (18) with Γ, a RCBF can be derived as

$$\tilde{u}(\bar{x}) \in \Big\{ u \in \mathbb{R} \,|\colon L_f h_1^i(\bar{x}) + L_{g1} h_1^i(\bar{x}) u + L_{g2} h_1^i(\bar{x}) \hat{d} + \lambda h_1^i(\bar{x}) \geq L_{g2} h_1^i(\bar{x}) \mathcal{L} \Big\}, \tag{19}$$

where $\mathcal{L} = [\Gamma, \Gamma]^\top$, $\tilde{u}(\bar{x})$ is the robust safety control set.

It is clear that $\tilde{u}(\bar{x})$ is a subset of $u(\bar{x})$. Compared to (18), (19) makes a relatively conservative restriction on control input u, so that a strict current constraint is guaranteed, even in the presence of disturbances.

Remark 2: Considering the fact that $L_{g2} h_1^1 = [0, 1]$ and $L_{g2} h_1^2 = [0, -1]$, it becomes evident that the safety control set $\tilde{u}(\bar{x})$ is only affected by the matched lumped disturbance d_2, and the mismatched lumped disturbance d_1 does not have an impact on it, thereby reducing the complexity involved in designing current constrained RCBF.

C. RCBF-Based SCGPC Design

To achieve the goal of integrating the GPC-based speed controller (10) and the current constrained RCBF (19) while preserving as much tracking performance as possible, a viable option is to make a minimal modification to the designed controller (10) based on the safety control set yielded by (19). Towards this end, the following optimization problem is formulated to generate a Lipschitz continuous controller

$$\begin{aligned} u^*(\bar{x}, t) &= \arg\min_{\tilde{u} \in \mathbb{R}} \|\tilde{u} - u_{\text{nom}}\|^2, \\ \text{s.t. } & L_f h_1^i(\bar{x}) + L_{g1} h_1^i(\bar{x}) \tilde{u} + L_{g2} h_1^i(\bar{x}) \hat{d} \\ & + \lambda h_1^i(\bar{x}) \geq L_{g2} h_1^i(\bar{x}) \mathcal{L} \end{aligned} \tag{20}$$

where $u_{\text{nom}} = u$ is the feedback control law yielded by (10).

Remark 3: In the existing approaches [13], [16], [19], both the CLF and CBF need to be designed. Then, by transforming the control sets generated by the CLF and CBF into a QP problem to achieve a safety-critical control. However, in this paper, an explicit speed controller has been provided in (10). Therefore, it is merely a matter of modifying the given baseline controller according to the safety control set generated by the current constrained RCBF, simplifying the optimization problem and providing a flexible control design framework.

Remark 4: As shown in (20), the designed RCBF requires only two parameters need to be adjusted. Firstly, Γ is usually chosen as a sufficiently large constant to compensate for the observation error. In practice, an effective way to obtain a satisfactory result is to make trials from large to small. Secondly, λ is used to tune the robustness of the RCBF against disturbances and uncertainties. The larger the λ, the stronger the robustness of the RCBF. It is usually selected from small to large according to the actual requirements.

The comprehensive control diagram of the proposed approach is depicted in Fig. 1.

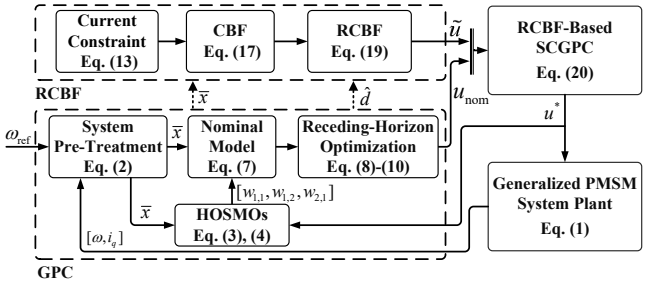

(a)

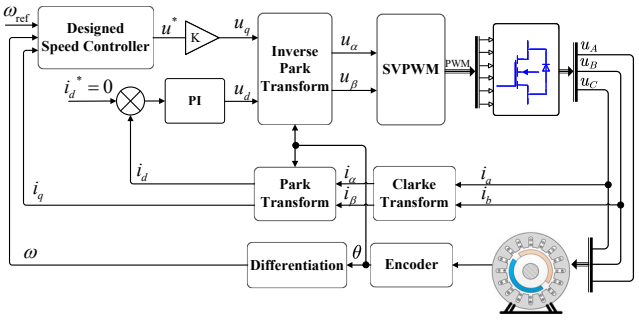

(b)

Fig. 1. Block diagram of the proposed control approach: (a) SCGPC block diagram, (b) System overview diagram.

V. Simulation Validations

In this section, a series of simulation programs based on MATLAB/Simulink tool are built to verify the effectiveness of the proposed control method. In the tests, the benchmark GPC [10] and the MPC based on DOB [21] are chosen as the comparison methods. The physical settings for the employed PMSM drives are given in Table I. Three different scenarios are tested, as listed in Table II.

TABLE I
PARAMETERS OF THE PMSM SYSTEM

Symbol	Quantity	Nominal values
n_p	Poles	4
R_s	Stator resistance	0.36 Ω
L_s	Stator inductance	2.0×10^{-4} H
ψ_f	Flux linkage	0.0064 Wb
J	Rotor inertia	7.066×10^{-6} kg·m^2
B_m	Viscous damping	2.637×10^{-6} N·m·s/rad
ω_{n}	Rated speed at V_{dc}	4107 rpm
$I_{\max}$	Rated current	7.1 A
V_{dc}	Bus voltage	24 V

TABLE II
DESIGN OF TEST CASES

Test Cases	t = 1 s	t = 1.5 s	Current constraint
Case 1	500 to 1500 rpm	$T_L = 0.027$ Nm	$I_{\max} = 1.0$ A
Case 2	500 to 2000 rpm	$T_L = 0.054$ Nm	$I_{\max} = 1.7$ A
Case 3	500 to 2500 rpm	$T_L = 0.081$ Nm	$I_{\max} = 2.5$ A

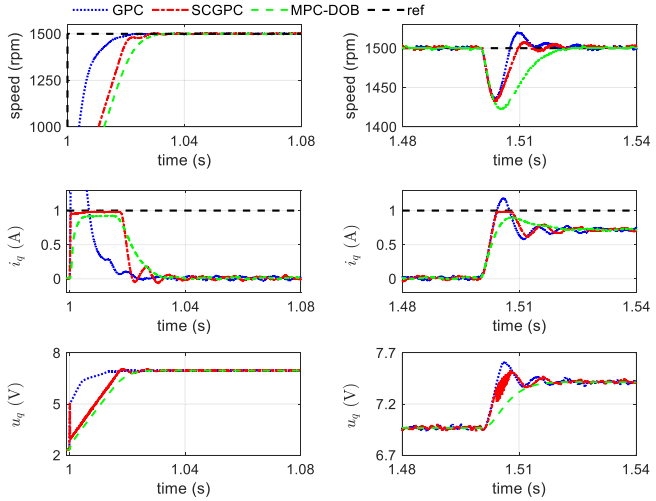

Fig. 2. Simulation results under Case 1.

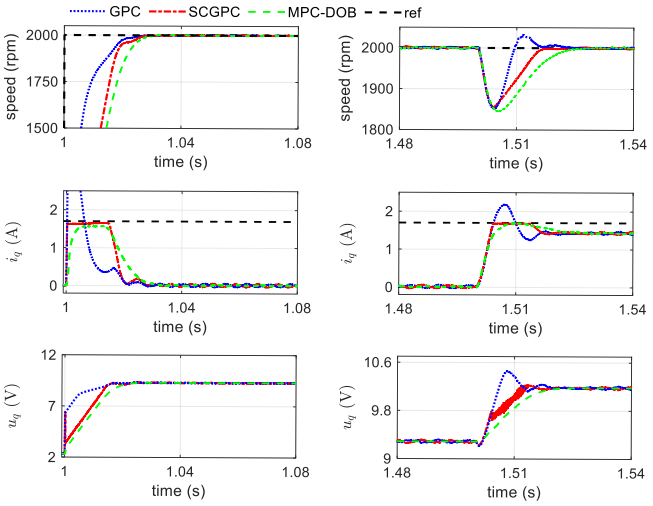

Fig. 3. Simulation results under Case 2.

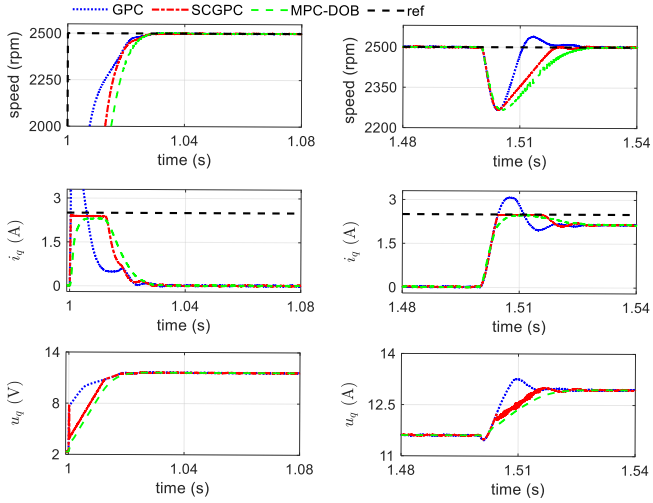

Fig. 4. Simulation results under Case 3.

To ensure a fair comparison, the selection criteria for the involved controller parameters take into the transient performance and disturbance rejection capability of the system in a comprehensive manner. The control parameters are set as follows: the benchmark GPC: $T = 0.003$, $\ell_{1,0} = 4$, $\ell_{1,1} = 2$, $\ell_{1,2} = 1.1$, $\rho_1 = 1500$, $\ell_{2,0} = 5$, $\ell_{2,1} = 2$, $\rho_2 = 7.5 \times 10^7$, $k_\omega^* = 10/3$, $k_{\mathrm{q}}^* = 2.5$; the proposed SCGPC: $\lambda = 5000$, $\mathcal{L} = [7 \times 10^3, 7 \times 10^3]^\top$, and the remaining parameters are the same as in the benchmark GPC; the DOB-based MPC: $T_{\mathrm{s}} = 5 \times 10^{-5}$, $N_{\mathrm{p}} = 20$, $N_{\mathrm{c}} = 3$; $Q = 1000 I_{20\times 20}$, $R = 1$, $a_{1,1} = 160$, $a_{1,2} = 6400$ for the GPIO1 [22]; $a_{2,1} = 120$, $a_{2,2} = 3600$ for the GPIO2;

As shown in Fig. 2, the peak current of the benchmark GPC far exceeds the predefined current limit for an optimal tracking objective. In contrast, the current curves of the proposed SCGPC and DOB-based MPC are well constrained to within 1A. Subsequently, as a normal load disturbance is applied to the system, a speed drop is suffered. It can be observed in Fig. 2 that although the benchmark GPC has the fastest recovery time, it violates the current safety constraint. Whereas the proposed SCGPC and the DOB-based MPC are still able to maintain the current within the safe margins, with an inevitable slight performance sacrifice.

As illustrated in Figs. 3 and 4, both the proposed SCGPC and the DOB-based MPC can ensure that the q-axis current remains within the specified safety margins during the transient stage. As for the benchmark GPC, the safety range is far exceeded, with higher peak current as the speed range becomes wider. Furthermore, it can be observed from Figs. 3 and 4 that all three methods exhibit similar speed drop in response to normal load. However, it is important to highlight that both the proposed SCGPC and the DOB-based MPC provide a rigorous guarantee of current safety constraint, whereas the benchmark GPC violates the constraint.

Meanwhile, the execution time of the three methods involved is evaluated via the Simulink Profiler tool of MATLAB,

TABLE III
COMPARISON OF CALCULATION EFFICIENCY

Controller	Total time (s)	Time of each control cycle (μs)
Benchmark GPC	5.8	9.06
Proposed SCGPC	10.11	15.8
MPC-DOB	58.84	90

as presented in Table III. It is evident that the one-step computation time of the DOB-based MPC is much greater than that of the benchmark GPC and SCGPC. However, it is important to note that both the SCGPC and the DOB-based MPC can effectively handle current constraint issues. Therefore, this confirms that the proposed SCGPC is more practical compared to the DOB-based MPC, particularly in scenarios involving microprocessors with limited computational power.

VI. EXPERIMENT RESULTS

In order to further validate the effectiveness of the proposed methodology, an experimental setup based on a digital signal processor (DSP) is constructed, on which comparative experiments are carried out.

A. Experimental Setup

The experimental setup includes of a F28379D control unit and two DRV8305 driver boards, both manufactured by Texas Instrument, as depicted in Fig. 5(a). Specifically, the F28379D is equipped with two central processing units (CPUs) operating at 200 MHz each. CPU1 is used to control the drive motor in speed mode. CPU2 is employed to operate the load motor in torque mode, generating the desired torque, which serves as the external load on the drive motor. Fig. 5(b) illustrates the comprehensive electrical connection diagram. The control algorithm is developed in MATLAB/Simulink through the model-based design method. The physical settings of the used motor are listed in Table I.

B. Performance Verification

To maintain consistency with the above simulation tests, the benchmark GPC [10] and the DOB-based MPC [21] are chosen as comparison methods for this experiment. Specifically, the control parameters are set as follows: the benchmark GPC: $T = 0.004$, $\ell_{1,0} = 12$, $\ell_{1,1} = 4.5$, $\ell_{1,2} = 2$, $\rho_1 = 4500$, $\ell_{2,0} = 7$, $\ell_{2,1} = 4$, $\rho_2 = 3.5 \times 10^8$, $k_\omega^* = 10/3$, $k_\mathrm{q}^* = 2.5$; the proposed SCGPC: $\lambda = 3000$, $\mathcal{L} = [1.5\times10^5, 1.5\times10^5]^\top$, and the remaining parameters are the same as in the benchmark GPC; the DOB-based MPC: $T_\mathrm{s} = 1\times10^{-4}$, $N_\mathrm{p} = 15$, $N_\mathrm{c} = 2$; $Q = 1000 I_{15\times15}$, $R = 1$, $a_{1,1} = 100$, $a_{1,2} = 2500$ for the GPIO1 [22]; $a_{2,1} = 70$, $a_{2,2} = 1225$ for the GPIO2; The sampling period of the benchmark GPC and the SCGPC is configured as 20 KHz, while the DOB-based MPC employs a sampling time of 10KHz due to complexity of the control algorithms. The experimental scenarios are listed in Table IV.

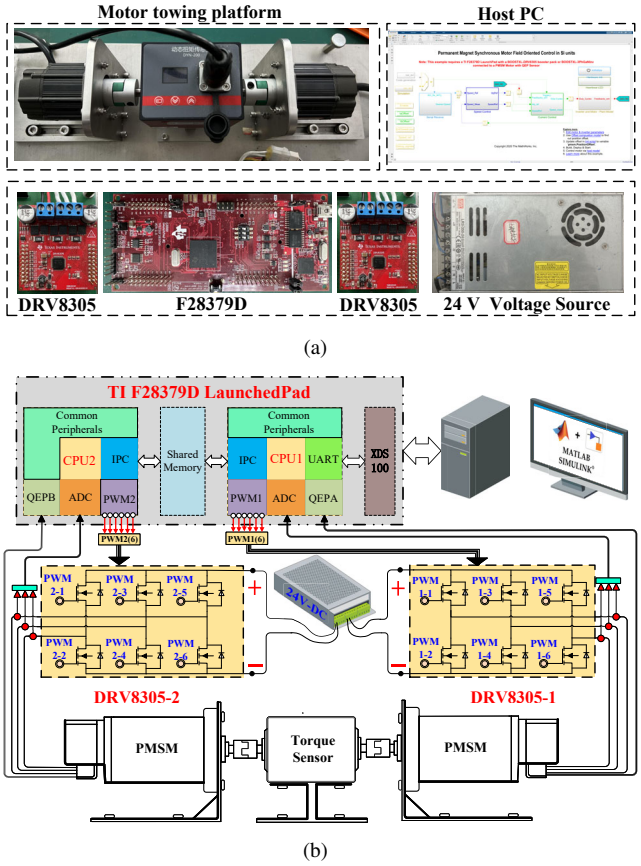

Fig. 5. Experimental setup: (a) Components composition, (b) Connection diagram.

TABLE IV
DESIGN OF TEST WORKING CONDITIONS

Test Cases	t = 8 s	t = 10 s	Current constraint
Case 1	500 to 1500 rpm	$T_L = 0.05$ Nm	$I_\mathrm{max} = 5$ A
Case 2	500 to 2000 rpm	$T_L = 0.10$ Nm	$I_\mathrm{max} = 6$ A
Case 3	500 to 3000 rpm	$T_L = 0.15$ Nm	$I_\mathrm{max} = 7$ A

1) Dynamic Performance: As shown in Fig. 6, with a speed change from 500 to 1500 rpm, although the benchmark GPC exhibits the fastest dynamic response for optimal performance, the peak current exceeds the predefined range. However, both the proposed SCGPC and the DOB-based MPC achieve to constrain the current within the specified range. Moreover, the transient performance of the proposed SCGPC is superior to that of the DOB-based MPC with a smaller period employed.

Figs. 7 and 8 depict the system response under Cases 2 and 3. It can be obviously observed that the current during the response is well constrained within the predetermined safe range under the SCGPC and the DOB-based MPC, while the proposed SCGPC has a faster response than the DOB-based MPC. However, the benchmark GPC leads to a larger peak current under a wide range of speed switching, far beyond the defined safe range, despite having a faster dynamic performance. The experimental results obtained are largely consistent with the above simulation tests.

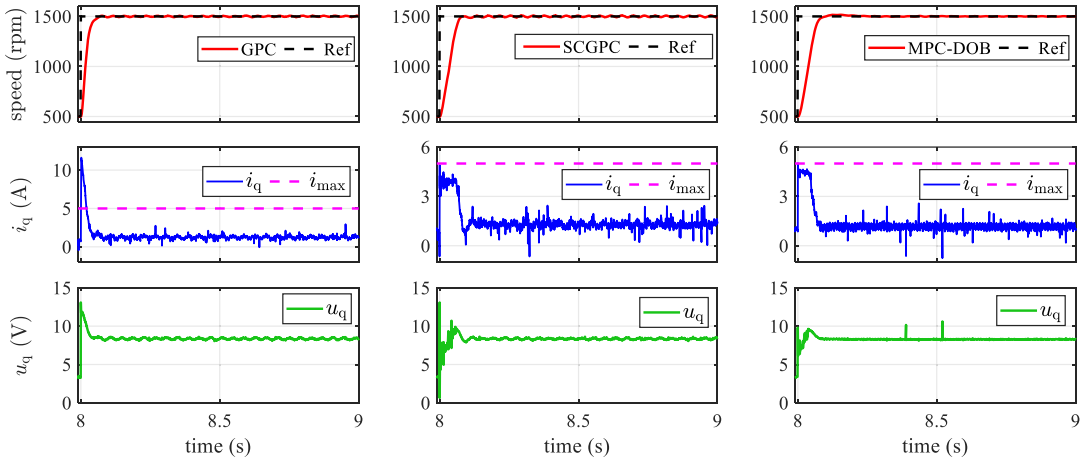

Fig. 6. System response curves of the different controllers under Case 1.

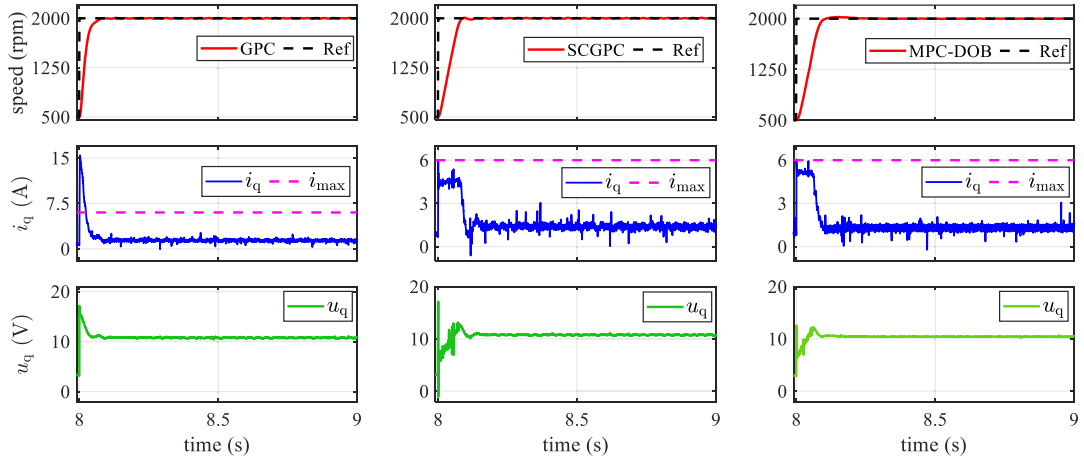

Fig. 7. System response curves of the different controllers under Case 2.

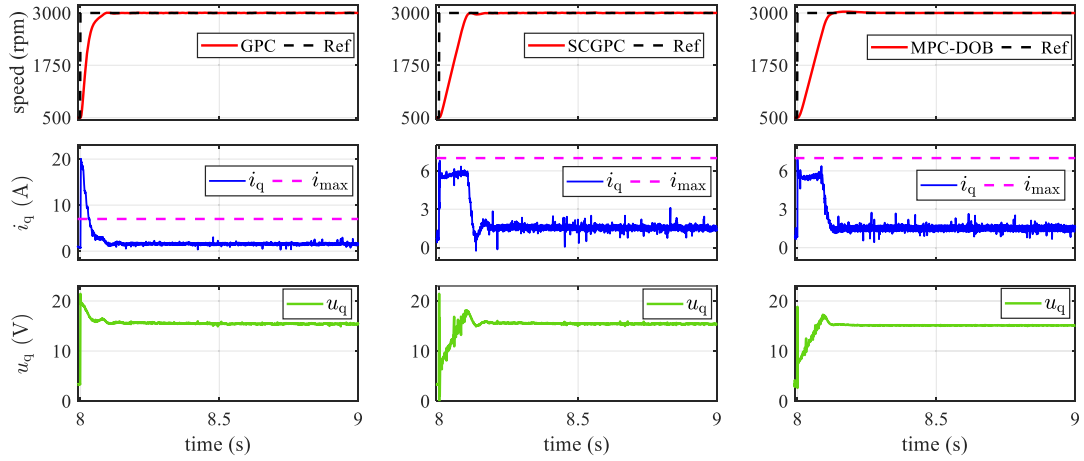

Fig. 8. System response curves of the different controllers under Case 3.

2) Robustness Against Disturbance: The system responses for the three considered control methods in the presence of various constant disturbances are illustrated in Fig. 9. It is readily apparent that both the benchmark GPC and the proposed SCGPC exhibit similar speed drops and performance recoveries in Cases 1-3. However, the DOB-based MPC suffers significant speed drop and slow performance recovery compared to the benchmark GPC and the SCGPC since a larger sampling time is implemented. This confirms that the proposed SCGPC offers an outstanding disturbance rejection capability.

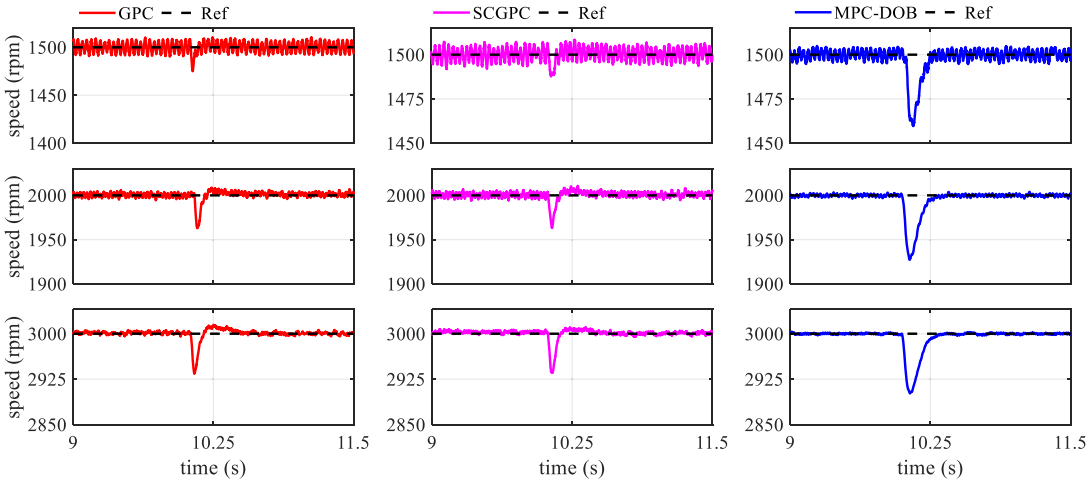

Fig. 9. System response curves of the different controllers in the presence of constant disturbance.

VII. Conclusion

This article has studied a novel SCGPC approach based on a RCBF for speed regulation of PMSM drives to solve the stator current constrained issue under a non-cascade structure. Meanwhile, the constraint deviation problem for CBF caused by system disturbances is considered by introducing a new RCBF. Subsequently, the GPC-based speed controller and the RCBF-based current constraint mechanism were integrated via an optimization problem. This achieves a possibility that the respective merits of MPC and GPC are well-merged while having a more efficient computational efficiency than MPC. Finally, the effectiveness of the proposed SCGPC method was verified by simulations and experiments.

References

[1] X. Liu, H. Chen, J. Zhao, and A. Belahcen, "Research on the performances and parameters of interior PMSM used for electric vehicles," *IEEE Transactions on Industrial Electronics*, vol. 63, no. 6, pp. 3533–3545, 2016.

[2] Q. Tan, X. Huang, L. Li, and M. Wang, "Magnetic field analysis and flux barrier design for modular permanent magnet linear synchronous motor," *IEEE Transactions on Industrial Electronics*, vol. 67, no. 5, pp. 3891–3900, 2019.

[3] J. Mao, S. Li, Q. Li, and J. Yang, "Design and implementation of continuous finite-time sliding mode control for 2-DOF inertially stabilized platform subject to multiple disturbances," *ISA Transactions*, vol. 84, pp. 214–224, 2019.

[4] J. Lara, J. Xu, and A. Chandra, "Effects of rotor position error in the performance of field-oriented-controlled PMSM drives for electric vehicle traction applications," *IEEE Transactions on Industrial Electronics*, vol. 63, no. 8, pp. 4738–4751, 2016.

[5] C. Dai, T. Guo, J. Yang, and S. Li, "A disturbance observer-based current-constrained controller for speed regulation of PMSM systems subject to unmatched disturbances," *IEEE Transactions on Industrial Electronics*, vol. 68, no. 1, pp. 767–775, 2020.

[6] Z. Cao, J. Mao, X. Dong, and C. Zhang, "Direct speed regulation for PMSM drive system via a generalized dynamic predictive control approach," in *2022 25th International Conference on Electrical Machines and Systems (ICEMS)*, 2022, pp. 1–6.

[7] M. M. Ismail, W. Xu, J. Ge, Y. Tang, A. K. Junejo, and M. G. Hussien, "Adaptive linear predictive model of an improved predictive control of permanent magnet synchronous motor over different speed regions," *IEEE Transactions on Power Electronics*, vol. 37, no. 12, pp. 15 338–15 355, 2022.

[8] X. Gao, M. Abdelrahem, C. M. Hackl, Z. Zhang, and R. Kennel, "Direct predictive speed control with a sliding manifold term for PMSM drives," *IEEE Journal of Emerging and Selected Topics in Power Electronics*, vol. 8, no. 2, pp. 1258–1267, 2019.

[9] Y. Zhang, D. Xu, and L. Huang, "Generalized multiple-vector-based model predictive control for PMSM drives," *IEEE Transactions on Industrial Electronics*, vol. 65, no. 12, pp. 9356–9366, 2018.

[10] J. Yang, W. X. Zheng, S. Li, B. Wu, and M. Cheng, "Design of a prediction-accuracy-enhanced continuous-time MPC for disturbed systems via a disturbance observer," *IEEE Transactions on Industrial Electronics*, vol. 62, no. 9, pp. 5807–5816, 2015.

[11] X. Dong, J. Mao, Y. Yan, C. Zhang, and J. Yang, "Generalized dynamic predictive control for nonlinear systems subject to mismatched disturbances with application to PMSM drives," *IEEE Transactions on Industrial Electronics*, vol. 71, no. 1, pp. 954–964, 2024.

[12] X. Tan, W. S. Cortez, and D. V. Dimarogonas, "High-order barrier functions: Robustness, safety, and performance-critical control," *IEEE Transactions on Automatic Control*, vol. 67, no. 6, pp. 3021–3028, 2021.

[13] A. D. Ames, J. W. Grizzle, and P. Tabuada, "Control barrier function based quadratic programs with application to adaptive cruise control," in *53rd IEEE Conference on Decision and Control*. IEEE, 2014, pp. 6271–6278.

[14] X. Xu, "Constrained control of input–output linearizable systems using control sharing barrier functions," *Automatica*, vol. 87, pp. 195–201, 2018.

[15] Q. Nguyen, A. Hereid, J. W. Grizzle, A. D. Ames, and K. Sreenath, "3D dynamic walking on stepping stones with control barrier functions," in *2016 IEEE 55th Conference on Decision and Control (CDC)*, 2016, pp. 827–834.

[16] A. D. Ames, S. Coogan, M. Egerstedt, G. Notomista, K. Sreenath, and P. Tabuada, "Control barrier functions: Theory and applications," in *2019 18th European Control Conference (ECC)*. IEEE, 2019, pp. 3420–3431.

[17] A. Levant, "Higher-order sliding modes, differentiation and output-feedback control," *International Journal of Control*, vol. 76, no. 9-10, pp. 924–941, 2003.

[18] W.-H. Chen, D. J. Ballance, and P. J. Gawthrop, "Optimal control of nonlinear systems: A predictive control approach," *Automatica*, vol. 39, no. 4, pp. 633–641, 2003.

[19] A. D. Ames, X. Xu, J. W. Grizzle, and P. Tabuada, "Control barrier function based quadratic programs for safety critical systems," *IEEE Transactions on Automatic Control*, vol. 62, no. 8, pp. 3861–3876, 2016.

[20] A. Isidori, *Nonlinear control systems: an introduction*. Springer, 1985.

[21] M. Zhou, X. Liu, and S. Li, "Composite single-loop model predictive control design for PMSM servo system speed regulation based on disturbance observer," in *2020 Chinese Control and Decision Conference (CCDC)*, 2020, pp. 2886–2892.

[22] Z. Wang, S. Li, J. Wang, and Q. Li, "Generalized proportional integral observer based backstepping control for DC-DC buck converters with mismatched disturbances," in *2016 IEEE International Conference on Industrial Technology (ICIT)*, 2016, pp. 1783–1789.